Acta Materialia 187 (2020) 19–28

Contents lists available at ScienceDirect

Acta Materialia

journal homepage: www.elsevier.com/locate/actamat

Full length article

# Room temperature deformation of 6*H*−SiC single crystals investigated by micropillar compression

Kyosuke Kishida[a,b,*], Yasuharu Shinkai[a], Haruyuki Inui[a,b]

[a] Department of Materials Science and Engineering, Kyoto University, Sakyo-ku, Kyoto 606-8501, Japan
[b] Center for Elements Strategy Initiative for Structural Materials (ESISM), Kyoto University, Sakyo-ku, Kyoto 606-8501, Japan

ARTICLE INFO

*Article History:*
Received 12 November 2019
Revised 9 January 2020
Accepted 11 January 2020
Available online 15 January 2020

*Keywords:*
Silicon carbide
Dislocations
Mechanical properties
Micropillar compression

ABSTRACT

The room-temperature plastic deformation behavior of 6*H*−SiC single crystals has been investigated by uniaxial compression of micropillar specimens as a function of crystal orientation and specimen size. Plastic flow is observed even at room temperature by basal and prism slip, latter of which have never been observed in the bulk. The CRSS values for basal and prism slip are as high as above 5 and 6 GPa at the specimen size of 5 $\mu$m, respectively, each of which increases with decreasing specimen size, following an inverse power-law relationship with a relatively small power-law exponent of ~0.10 and ~0.21, respectively. The CRSS values for basal slip are not virtually affected by the existence of basal dislocations introduced at 1300 °C prior to micropillar compression tests at room temperature. The majority of basal dislocations observed after micropillar compression are perfect (undissociated) screw dislocations, and they are considered to be introduced in the shuffle-set plane during micropillar testing, unlike widely dissociated dislocations introduced in the glide-set plane in the bulk during high-temperature deformation. Prism dislocations are observed also to glide as perfect (undissociated) dislocations and tend to align strongly along their screw orientation. The fracture toughness values are estimated to be 1.37 ± 0.13 and 1.57 ± 0.13 MPa $m^{1/2}$ by three-point bend tests for chevron-notched single crystalline specimens with a notch plane being parallel to (0001) and $\{01\bar{1}0\}$ planes, respectively.



## 1. Introduction

Plastic deformation of single crystals of various semiconducting materials, such as Si, Ge, GaAs, InP and SiC has been the subject of extensive studies, revealing that these semiconducting materials are generally brittle at ambient temperatures and are plastically deformable by dislocation glide only at high temperatures under uniaxial loading conditions [1–9]. However, in these semiconducting materials, dislocation activation on octahedral planes for cubic materials or basal planes for hexagonal materials has been observed not only at high temperatures but also at ambient temperatures if premature fracture is successfully suppressed by the application of very high hydrostatic pressure or under indentation conditions [10–16]. These are clear indication that these semiconducting materials are not intrinsically brittle but some external factors may be responsible for the serious difficulty in activating slip systems at ambient temperature under uniaxial loading conditions.

For hexagonal polytypes of SiC, i.e., 4*H*− and 6*H*−SiC, basal slip is the easiest operative deformation mode at temperatures above room temperature. The critical resolved shear stress (CRSS) value for basal slip exhibits a very strong temperature dependence, which is generally interpreted to originate from the Peierls mechanism [8,9]. Pirouz and his coworkers have proposed that the thermal activation process that controls the glide of basal dislocations varies with temperature based on the analysis of their activation parameters and dislocation microstructures by transmission electron microscopy (TEM) [9,17–19]. At high temperatures above 1100 °C, basal dislocations are completely dissociated into two Shockley partials with a very low stacking fault energy of about 2.5 mJ/$m^2$ [10]. At an intermediate temperature range below 1100 °C, only leading partial dislocations can glide so that wide stacking faults with various widths are formed behind with the anchored trailing partials [18]. These observations indicate that basal dislocations in hexagonal polytypes of SiC prefer to glide in the glide-set plane at high temperatures as in the case of the other semiconducting materials with the cubic structures such as Si, Ge and GaAs [5,12,15,17]. At much lower temperature region around room temperature, the coexistence of perfect (undissociated) dislocations and dissociated dislocations has been observed in 4*H*−SiC deformed by compression under confining pressure or by

* Corresponding author at: Department of Materials Science and Engineering, Kyoto University, Sakyo-ku, Kyoto 606-8501, Japan.
*E-mail address:* kishida.kyosuke.6w@kyoto-u.ac.jp (K. Kishida).

https://doi.org/10.1016/j.actamat.2020.01.027

indentation tests [20]. Based on the observations of perfect (undissociated) dislocations, it has been proposed that basal dislocations are nucleated as perfect dislocations in the shuffle-set plane as in the case of Si deformed at low temperature under very high applied stress [14,15,21]. In addition, prism slip in 6*H*−SiC has been reported to operate by indentation at room temperature while this is not the case for other testing conditions including uniaxial compression [12]. However, details about the room-temperature deformation behavior and mechanisms of hexagonal SiC, in particular the CRSS values and their controlling mechanism for basal and prism slip systems, have not been fully clarified yet.

Recently, micropillar compression testing, which was originally introduced by Uchic et al. to investigate the mechanical response of various metallic materials with the FCC or BCC structures at size-scales of tens of micrometers or smaller [22], has been found to be a very powerful tool in studying the deformation behavior of brittle materials at temperatures far below their ductile to brittle transition temperatures [22–35]. Micheler et al. were the first who applied the method to GaAs and Si single crystals with cubic crystal structures and successfully confirmed their relatively large room-temperature plastic deformability comparable to that observed for single crystalline micropillar specimens of conventional FCC and BCC metals [23,24,26]. Following their studies, deformation behavior of semiconductors, ceramics (borides, carbides, oxides) and intermetallic compounds has been studied by the micropillar compression method [25–35]. We have investigated the deformation behavior of various hard and brittle materials including transition-metal silicides, MAX phase compounds and various intermetallic phases with complex crystal structures by utilizing the micropillar compression method, and have confirmed that most of them are plastically deformable even at room temperature if the specimen size is reduced to the micrometer size [36–40]. In our studies, we have utilized micropillar specimens in a rectangular parallelepiped shape, instead of cylindrical ones commonly used in most of the early studies, so as to facilitate slip system identification for hard and brittle materials with hexagonal, tetragonal and lower symmetry, and have successfully identified many operative deformation modes that had never been confirmed with confidence [36–40]. Very recently, the micropillar compression method has also been applied to submicron-sized cylindrical specimens of 6*H*−SiC and 4*H*−SiC single crystals and the activation of basal slip and the possible occurrence of deformation-induced phase transformation at room temperature has been reported [41,42]. These previous studies clearly indicate that the micropillar compression method is actually capable of investigating room-temperature deformation behavior of hexagonal SiC.

In the present study, we investigate the plastic deformation behavior of single crystals of 6*H*−SiC in compression as a function of crystal orientation at room temperature, paying special attention to operative slip systems (other than basal slip), their CRSS values and dislocation dissociation schemes to identify either the shuffle- or glide-set for basal dislocation.

## 2. Experimental procedure

A bulk single crystal of n-type SiC with the 6*H*-type crystal structure (*hP*12, Space group: $P6_3mc$ (#186), $a$ = 0.3073 nm, $c$ = 1.5117 nm) was purchased from TanKeBlue semiconductor Co., Ltd. The micropipe density in the single crystal of the semiconductor-grade was estimated to be as low as 11 $cm^{-2}$. Orientations of the bulk single crystals were analyzed by the X-ray Laue back-reflection method. Two loading-axis orientations, [10 $\bar{5}$ $\bar{5}$ 3] (45° from both *a*- and *c*-axes) and [2 $\bar{1}$ $\bar{1}$ 0], were selected for micropillar compression tests. Oriented bulk specimens in a rectangular parallelepiped shape (approximate dimensions: 6 × 2 × 1 $mm^3$) were cut from the bulk single crystals so that a pair of top and bottom surfaces were perpendicular to the loading axis, and a pair of side surfaces were parallel to (0 1 $\bar{1}$ 0). Each of the oriented bulk specimens was kept fixed on a cylinder-shaped specimen mount (12.5 mm in diameter and 5 mm in height) during the following processes so as to minimize possible misalignment of the top surface. The top surfaces were mechanically polished and finished with diamond paste to mirror finish. Micropillar specimens with a square cross section having an edge length $L$ ranging from 1 to 7 $\mu$m and an aspect ratio of about 1:3 were fabricated on the mirror-finished top surfaces by the focused-ion beam (FIB) technique. Micropillar compression tests were carried out at room temperature under the displacement-rate-controlled mode at a nominal strain rate of 1 × $10^{-4}$/s with an Agilent Technologies Nano Indenter G200 nanomechanical tester equipped with a flat-punch diamond tip. Microstructures of micropillar specimens before and after compression tests were examined by scanning electron microscopy (SEM) with a JEOL JSM-7001FA electron microscope equipped with a field-emission gun. Dislocation structures in deformed micropillars were investigated by transmission electron microscopy (TEM) with a JEOL JEM-2000FX electron microscopes operated at 200 kV. Specimens for TEM observations were prepared by the FIB-SEM in-situ lift-out technique with a FEI Quanta 3D 200i Dual-Beam system equipped with an Omniprobe nanomanipulator.

In order to investigate the influence of pre-strains on the subsequent micropillar deformation behavior, basal dislocations were introduced in a bulk (millimeter-sized) single crystal specimen (2 × 2 × 6 $mm^3$) by uniaxial compression along [10 $\bar{5}$ $\bar{5}$ 3] to about 7% plastic strain at 1300 °C at a strain rate of 2.7 × $10^{-4}$ /s. Micropillar specimens were then fabricated from the central part of the pre-strained specimen and were tested in compression, followed by deformation microstructure observations by SEM and TEM, as described above.

Fracture toughness was measured by single-cantilever bend testing on chevron-notched micro-beam specimens ($l$: 12 $\mu$m, $W$: 4.5 $\mu$m, $B$: 3 $\mu$m; see the inset of Fig. 7) with an Agilent Technologies Nano Indenter G200 nanomechanical tester equipped with a Berkovich indenter tip at room temperature and at a constant displacement rate of 5 nm $s^{-1}$. Two notch planes, (0001) and (0 1 $\bar{1}$ 0), were selected, while the loading-axis direction was set parallel to [2 $\bar{1}$ $\bar{1}$ 0]. The fracture toughness value, $K_{IC}$ was evaluated from the maximum load ($P_{max}$) with numerical analysis using the equations proposed by Deng et al. [39,43] The details of the micro-beam specimens and the evaluation method for $K_{IC}$ are detailed in our previous paper [39].

## 3. Results

### 3.1. Stress–strain behavior and slip trace observation

Fig. 1(a) and (b) shows typical stress–strain curves for micropillar specimens with the [10 $\bar{5}$ $\bar{5}$ 3] and [2 $\bar{1}$ $\bar{1}$ 0] orientations tested in compression. Most compression tests, including those presented in Fig. 1 were stopped before failure occurs for the ease of slip trace analysis. Most specimens exhibit an abrupt transition of elastic to plastic flow with the occurrence of a small strain burst that appears as a flat portion in the stress–strain curve immediately after the elastic region, regardless of the loading-axis orientation. Arrows in Fig. 1 indicate yield point determined from the elastic limit, most of which were detected from the first detectable strain burst. Yield stress values obtained for micropillars with the [10 $\bar{5}$ $\bar{5}$ 3] and [2 $\bar{1}$ $\bar{1}$ 0] orientations are extremely high so as to exceed 11 GPa and 13 GPa, respectively, exhibiting a tendency to increase with the decrease in the specimen size (edge length $L$).

For the [10 $\bar{5}$ $\bar{5}$ 3] orientation, intense deformation markings are observed in a very localized manner along the trace of (0001) basal planes on the (2 $\bar{1}$ $\bar{1}$ $\bar{1}$0) side surface, while they are faint on the (0 1 $\bar{1}$ 0) side surface (Fig. 2(a)) for all specimens. The faint deformation markings

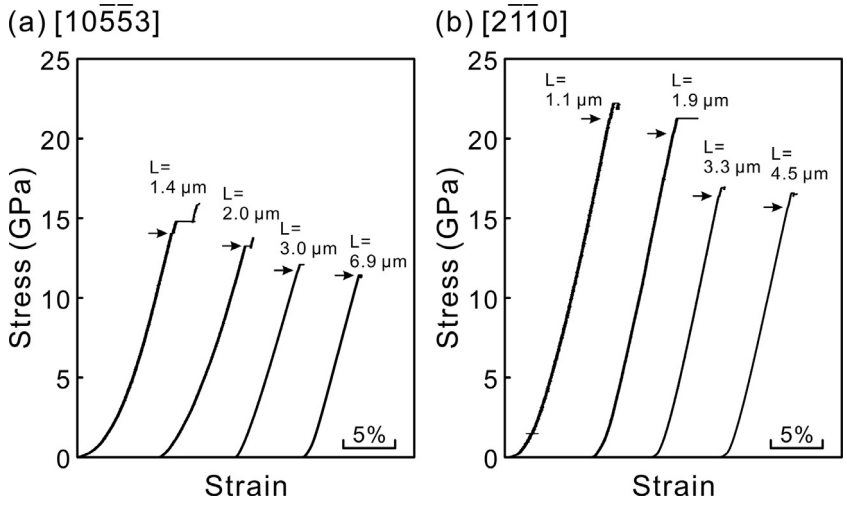


**Fig. 1.** Typical stress–strain curves obtained by micropillar compression tests for 6*H*–SiC single crystals with the (a) [10$\bar{5}\bar{5}$3] and (b) [2$\bar{1}\bar{1}$0] orientations. Arrows indicate the yield points determined from the elastic limit.

indicate that the slip direction is contained on the (0 1 $\bar{1}$ 0) side surface. The occurrence of (0001)[2 $\bar{1}$ $\bar{1}$ 0] basal slip is thus confirmed from trace analysis regardless of the specimen size. For bulk single crystals, (0001)[2 $\bar{1}$ $\bar{1}$ 0] basal slip is observed only above 550 °C in uniaxial compression [8,9]. For the [2 $\bar{1}$ $\bar{1}$ 0] orientation, intense deformation markings are observed again in a very localized manner along the trace of (1 0 $\bar{1}$ 0) prism planes on the (0 1 $\bar{1}$ 0) side surface, while they are faint on the (0001) side surface (Fig. 2(a)) for all specimens. These observations indicate the occurrence of (10 $\bar{1}$ 0)[1 $\bar{2}$ 10] slip. For bulk single crystals, (10 $\bar{1}$ 0)[1 $\bar{2}$ 10] slip has never been observed in uniaxial compression at any temperatures.

### 3.2. Dislocation structures

Fig. 3(a) shows a TEM weak-beam image of dislocation structure formed by (0001)[2 $\bar{1}$ $\bar{1}$ 0] basal slip in a [10 $\bar{5}$ $\bar{5}$ 3] -oriented micropillar specimen. The thin foil was cut parallel to the (2 $\bar{1}$ $\bar{1}$ $\bar{1}$0) side surface of a [10 $\bar{5}$ $\bar{5}$ 3] -oriented micropillar specimen shown in Fig. 2(a). A very high density of basal dislocations is observed to form a bright band region extending along the trace of (0001), which corresponds to shear deformation to form the step in the SEM images (Fig. 2(a)). Most dislocations in the band are found to align along [2 $\bar{1}$ $\bar{1}$ 0], i.e. along their screw orientation and they appear as perfect (undissociated dislocations without any significant dissociation) (Fig. 3(b)). In addition to these undissociated dislocations forming a band, some groups of dislocations are observed in the vicinity of the dislocation band. In these dislocation groups, perfect (undissociated) dislocations are seen to coexist with dissociated dislocations with a tendency to align along either the screw or 30°-orientations (Fig. 4).

The dissociation scheme of these $a/3$[2 $\bar{1}$ $\bar{1}$ 0] dissociated and undissociated dislocations was investigated by weak-beam imaging as shown in Fig. 4(a)–(e). The dislocations marked A in Fig. 4(a) (imaged with the reflection vector $\mathbf{g}=\bar{1}\ 10\ \bar{2}$), Fig. 4(b) ($\mathbf{g}=\bar{1}\ \bar{1}\ 20$), Fig. 4(c) ($\mathbf{g}=\bar{1}\ 2\ \bar{1}\ 0$) and Fig. 4(d) ($\mathbf{g}=\bar{1}\ 0\ 1\ \bar{2}$), are invisible when imaged with $\mathbf{g}=0\ 1\ \bar{1}\ \bar{2}$ (Fig. 4(e)). The dislocations marked A are thus determined to be undissociated dislocations with the Burgers vector $\mathbf{b}=a/3[2\ \bar{1}\ \bar{1}\ 0]$. The dislocations marked B visible on the left side of a stacking fault in Fig. 4(b) ($\mathbf{g}=\bar{1}\ \bar{1}\ 20$) are invisible when imaged with $\mathbf{g}=\bar{1}\ 2\ \bar{1}\ 0$ (Fig. 4(c)). The Burgers vector of the partial dislocations marked B is thus inferred to be $a/3[1\ 0\ \bar{1}\ 0]$. The dislocations marked C visible on the right side of a stacking fault in Fig. 4(c) ($\mathbf{g}=\bar{1}\ 2\ \bar{1}\ 0$) are invisible when imaged with $\mathbf{g}=\bar{1}\ \bar{1}\ 20$ (Fig. 4(b)),

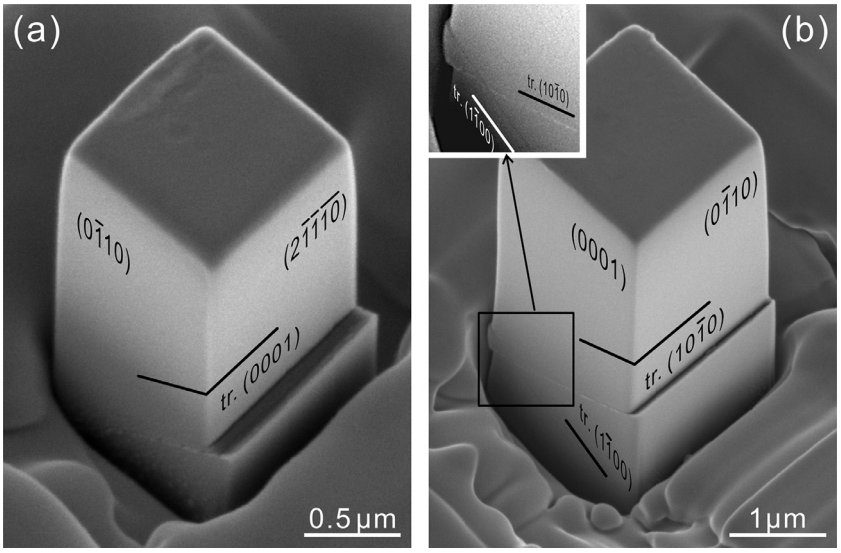


**Fig. 2.** Deformation markings observed on two orthogonal surfaces of 6*H*–SiC single crystalline micropillars with the (a) [10$\bar{5}\bar{5}$3] and (b) [2$\bar{1}\bar{1}$0] orientations.

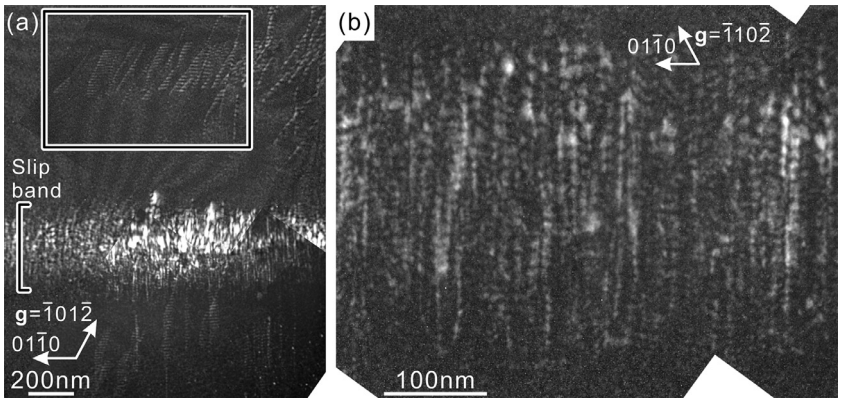


**Fig. 3.** (a) A weak-beam image of deformation microstructure in a [10$\bar{5}\bar{5}$3] -oriented micropillar specimen deformed by basal slip and (b) a magnified view of the slip band region in (a).

indicating that the Burgers vector of the partial dislocation C is $a/3[1\,\bar{1}\,0\,0]$. As marked with arrowheads in the weak beam images (Fig. 4(a)–(d)) and in a schematic illustration (Fig. 4(f)), some dislocation nodes are formed so that a perfect dislocation A is connected with two different partial dislocations B and C with a stacking fault in between. This clearly indicates that a $a/3[2\,\bar{1}\,\bar{1}\,0]$ perfect dislocation dissociates into two Shockley partials with Burgers vectors of $a/3[1\,0\,\bar{1}\,0]$ and $a/3[1\,\bar{1}\,0\,0]$ according to the following dissociation scheme.

$$a/3\left[2\,\bar{1}\,\bar{1}\,0\right] \rightarrow a/3\left[1\,0\,\bar{1}\,0\right] + a/3\left[1\,\bar{1}\,0\,0\right] \quad (1)$$

The stacking fault energy estimated from the observed dissociation width (18–56 nm for the 30°-orientation) is 8 ∼ 24 mJ/m$^2$, which is much higher than that (2.5 ± 0.9 mJ/m$^2$) previously reported for 6*H*–SiC deformed in compression at 1520 °C [12].

The coexistence of perfect (undissociated) and dissociated dislocations has not been observed in bulk-sized single crystals deformed in compression above 1100 °C, in which all basal dislocations with $\mathbf{b} = a/3[2\,\bar{1}\,\bar{1}\,0]$ are reported to widely dissociate into two Shockley partials [12]. The coexistence of perfect (undissociated) and dissociated dislocations is similarly observed only in 4*H*–SiC single crystals deformed at 150 °C under hydrostatic pressure of 5 GPa [20], in which dislocations are concluded to be nucleated as perfect (undissociated) dislocations of the shuffle type.

Shear deformation by $(1\,0\,\bar{1}\,0)[1\,\bar{2}\,1\,0]$ prism slip is also found to be extremely localized as seen in Fig. 2(b), and consequently, it is quite difficult to image individual dislocations in the shear localized region under the weak-beam imaging conditions. As in the case of the basal slip in the [10$\bar{5}\bar{5}$3] oriented-micropillar, some groups of dislocations with a relatively low density, which are suitable for weak-beam imaging, are found to exist in the vicinity of the shear localized region. Fig. 5 shows a TEM weak-beam image of a dislocation structure formed by $(1\,0\,\bar{1}\,0)[1\,\bar{2}\,1\,0]$ prism slip in the vicinity of the shear localized region. The thin foil was cut parallel to the $(0\,1\,\bar{1}\,0)$ side surface of a $[2\,\bar{1}\,\bar{1}\,0]$ -oriented micropillar. Most dislocations are confirmed to be screw dislocations with the Burgers vector of $a/3[1\,\bar{2}\,10]$ $a/3[1\,\bar{2}\,10]$ and they do not dissociate into partial dislocations, at least at the spatial resolution of weak-beam imaging. $\{1\,0\,\bar{1}\,0\}\langle 1\,\bar{2}\,1\,0\rangle$ prism slip has never been observed in bulk-sized specimens deformed in compression at any temperatures, except that it has been reported to be introduced by indentation at room temperature [12].

### 3.3. *Effects of pre-straining*

For the [10 $\bar{5}$ $\bar{5}$ 3] orientation, influences of pre-straining on the micropillar deformation behavior were investigated, as summarized

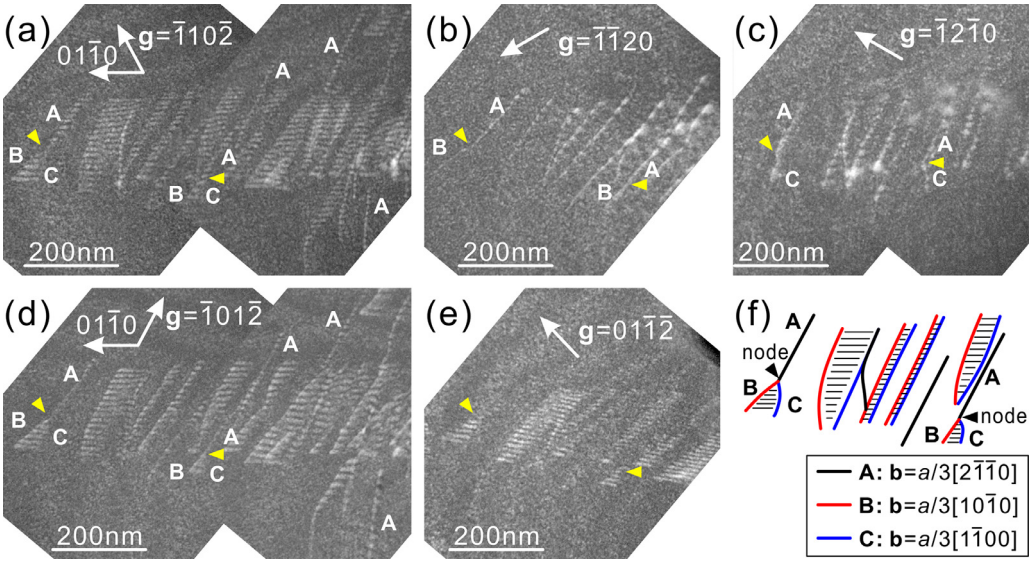


**Fig. 4.** (a)–(e) Contrast analysis and (f) a schematic illustration of dislocation structures on basal planes in the area marked in (a).

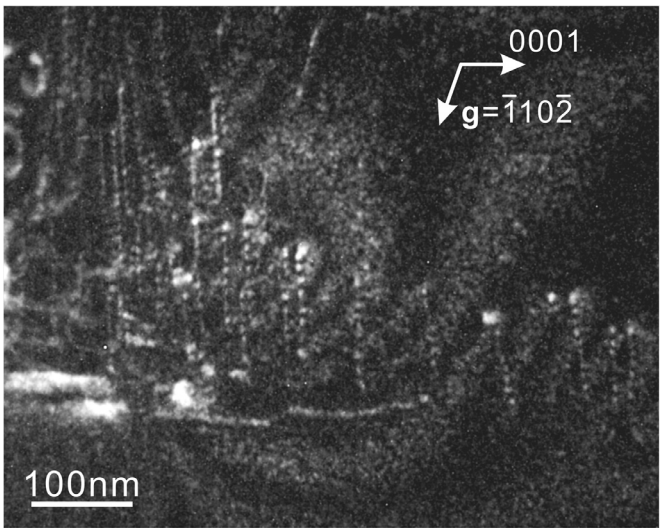


**Fig. 5.** A weak image of prism dislocations in a [$2\bar{1}\bar{1}0$] -oriented micropillar specimen deformed in compression.

in Fig. 6. This was done because there is a possibility that dislocations carrying the plastic strain by basal slip during micropillar compression testing are different from those carrying the plastic strain by basal slip during bulk compression testing in terms of how dislocations with $\mathbf{b} = a/3[1\,\bar{2}\,1\,0]$ are dissociated on basal planes (undissociated or widely-dissociated). A pre-strain of 7% was introduced in a bulk-sized single crystals with the [10 $\bar{5}$ $\bar{5}$ 3] orientation by uniaxial compression at 1300 °C. The stress–strain curve obtained for the pre-straining experiment exhibits a sharp yield drop followed by a gradual increase in the flow stress with increasing strain (Fig. 6(a)). The occurrence of a yield drop, which has commonly been observed for covalent semiconductors [6], suggests a very low dislocation density in as-grown single crystals used in the present study. The CRSS value estimated from the upper yield point is 14.2 MPa, the value of which coincides well with that (~16 MPa) previously reported [8]. The bulk-sized specimen was pre-strained up to about 7% plastic strain and then the central part of the specimen was used for the subsequent micropillar compression testing. As seen in Fig. 6(b) and (c), no apparent differences are noted in the characteristics of stress–strain behavior, yield stress and deformation microstructure for virgin and pre-strained micropillar specimens with the [10 $\bar{5}$ $\bar{5}$ 3] orientation. This indicates that (0001)[2 $\bar{1}$ $\bar{1}$ 0] basal slip activated in [10 $\bar{5}$ $\bar{5}$ 3] -oriented micropillars at room temperature are not influenced much by (widely-dissociated) basal dislocations introduced by 7% pre-strain at 1300 °C. Possible reasons for this will be discussed later in the discussion section.

### 3.4. Fracture toughness

Typical load-displacement curves obtained in three-point bend tests for chevron-notched micro-beam specimens with a notch plane parallel to either (0001) or (0 1 $\bar{1}$ 0) are shown in Fig. 7. All tested micro-beam specimens fractured without exhibiting any detectable plastic flow. Microstructure observations have confirmed the occurrence of cleavage fracture with a very flat fracture surface parallel to the chevron-notch plane of either (0001) or (0 1 $\bar{1}$ 0). The values of fracture toughness, $K_{IC}$ evaluated using Eqs. (1, 2) in Ref. [39] is 1.37 ± 0.13 and 1.57 ± 0.13 MPa $m^{1/2}$ for the (0001)- and (0 1 $\bar{1}$ 0) -notched micro-beam specimens, respectively. These values of fracture toughness $K_{IC}$ are in good agreement with that (1.80 ± 0.26 MPa $m^{1/2}$, (0001)-notched) obtained by a double cantilever beam compression tests of micron sized specimens [44] and those (1.9–2.5 MPa $m^{1/2}$) evaluated for the oriented-surfaces of bulk single crystals by an indentation method [45].

## 4. Discussion

### 4.1. Critical resolved shear stress

Critical resolved shear stresses (CRSSs) for (0001)[2 $\bar{1}$ $\bar{1}$ 0] basal slip and (1 0 $\bar{1}$ 0)[1 $\bar{2}$ 1 0] prism slip calculated with yield stress values and Schmid factors (0.5 and 0.433) are plotted respectively in Fig. 8 (a) and (b) as a function of the specimen size (edge length $L$). The CRSS values for each slip system follow an inverse power-law relationship with the specimen size $L$, i.e. $\tau_{CRSS} \propto L^{-n}$, where $n$ is a power-law exponent. For (0001)[2 $\bar{1}$ $\bar{1}$ 0] basal slip, the CRSS values and their size dependence for virgin and pre-strained specimens are very similar, indicating that the influence of the dislocations introduced in the bulk at 1300 °C on the onset of plastic deformation of micropillar specimens is virtually negligible. The $n$ values are estimated to be about 0.10 and 0.21 for (0001)[2 $\bar{1}$ $\bar{1}$ 0] basal slip and (1 0 $\bar{1}$ 0)[1 $\bar{2}$ 1 0] prism slip, respectively. These $n$ values are much smaller than those reported for conventional BCC metals (0.2–0.5) and FCC metals (0.5–1.0) and are close to those (0.16–0.22) observed for a hard intermetallic compound of $Mo_5SiB_2$ with the $D8_l$ structure [39].

According to previous studies on micropillar deformation for FCC and BCC metals, the CRSS values extrapolated from the power-law

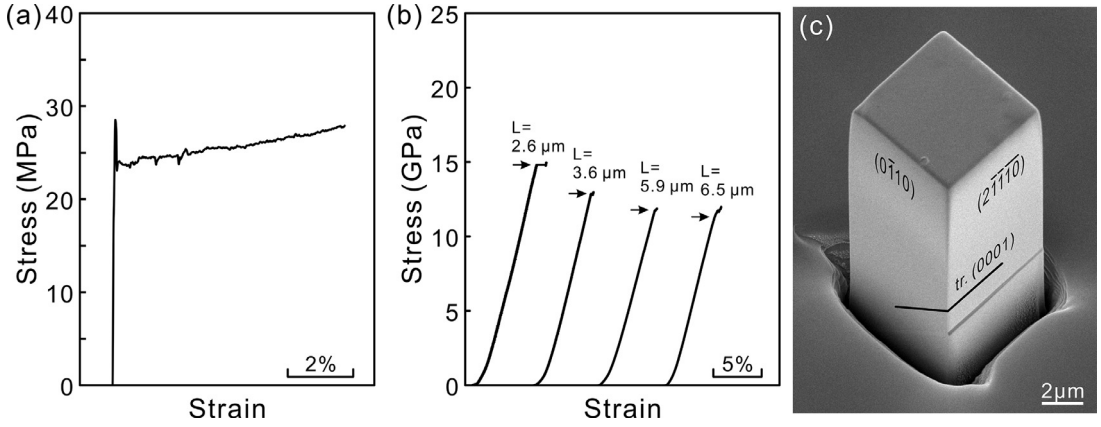


**Fig. 6.** (a) Stress–strain curve for a pre-straining compression test of a bulk-sized single crystal with the [10$\bar{5}\bar{5}$3] orientation deformed at 1300 °C, (b) typical stress–strain curves and (c) deformation microstructure obtained by micropillar compression tests for pre-strained 6*H*–SiC single crystals with the [10$\bar{5}\bar{5}$3] orientation.

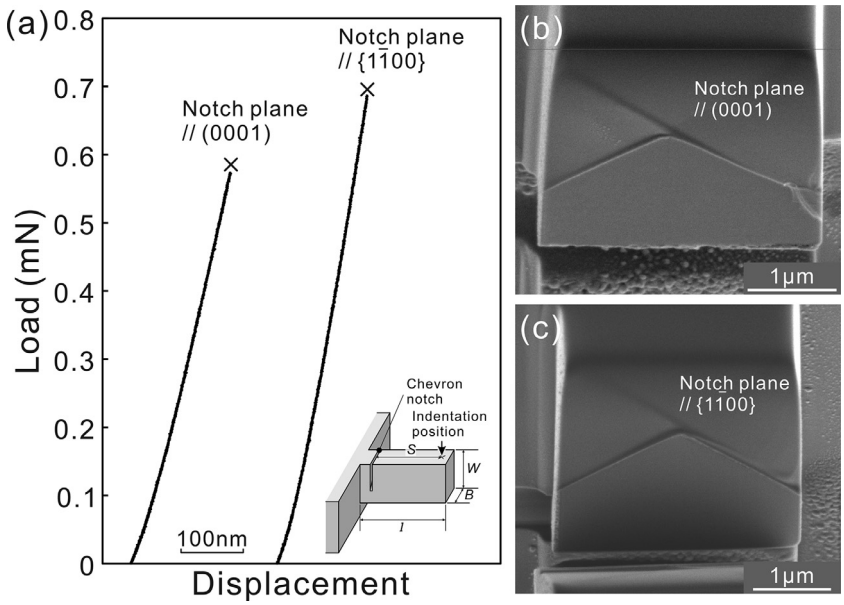


**Fig. 7.** (a) Typical load-displacement curves obtained in three-point bend test for chevron-notched micro-beam specimens and (b) and (c) SEM secondary electron images of the fracture surfaces of micro-beam specimens with a notch-plane parallel to (b) (0001) basal plane and (c) {1$\bar{1}$00} prism plane.

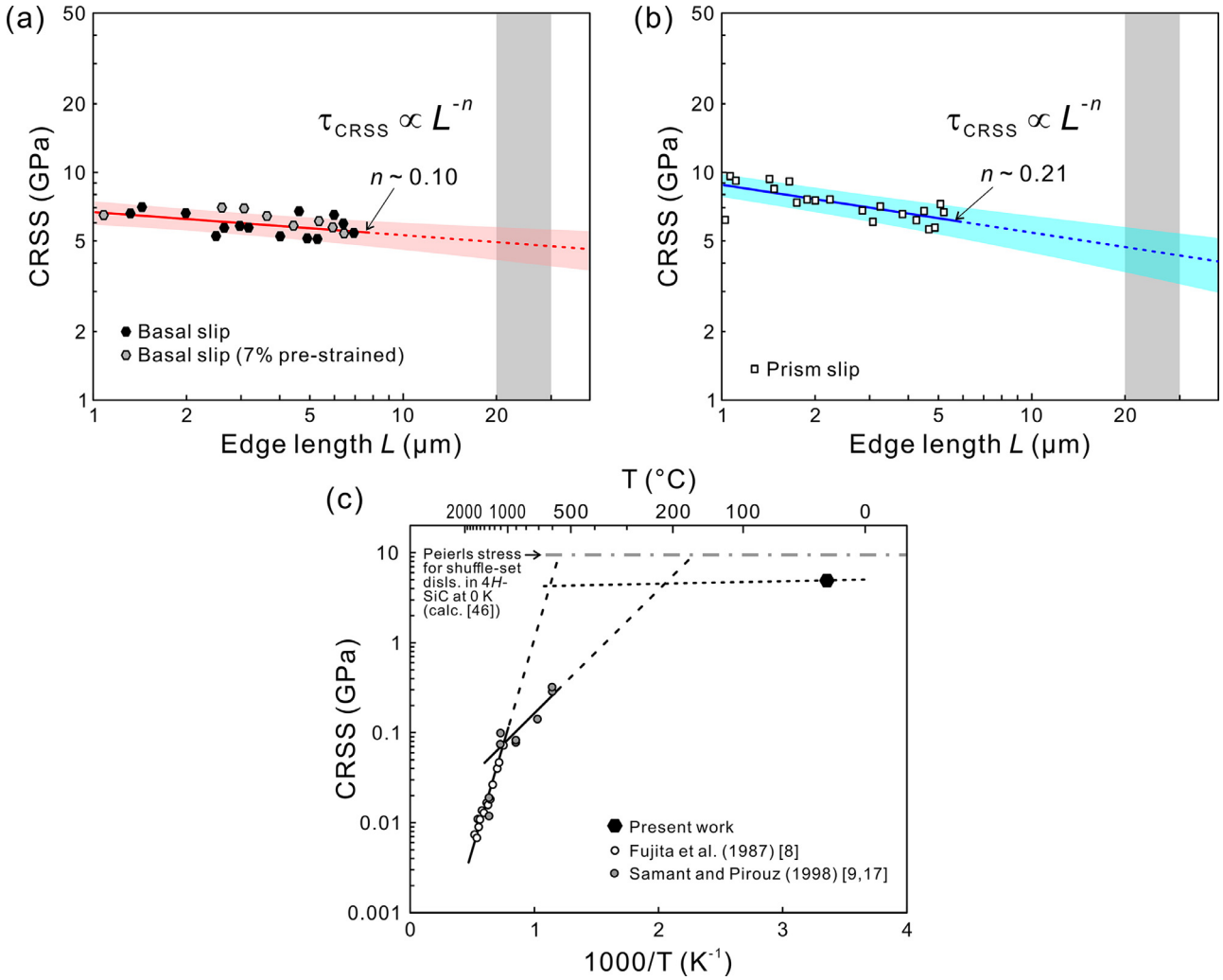


**Fig. 8.** (a) Specimen size dependence of CRSS values for basal and prism slip and (b) comparison of estimated bulk CRSS at room temperature with those at high temperatures reported in literatures [8,9,17].

curves of micropillar specimens of FCC and BCC metals coincide with those obtained by mechanical tests of the corresponding bulk-sized single crystals when the size of micropillar specimens is in the range of 20–30 $\mu$m [46,47]. Based on this, we can deduce the bulk CRSS values at room temperature for $(0001)\langle 2\,\bar{1}\,\bar{1}\,0\rangle$ basal and $\{0\,1\,\bar{1}\,0\}\langle 2\,\bar{1}\,\bar{1}\,0\rangle$ prism slip in 6*H*–SiC to be 4.8 ± 1.0 GPa and 4.5 ± 1.2 GPa, respectively. The bulk CRSS value is estimated as an average value from the extrapolated values at $L$ = 20 and 30 $\mu$m and the errors are estimated based on the standard deviation of fitting parameters for the power-law relationship. Surprisingly, the CRSS values for $(0001)\langle 2\,\bar{1}\,\bar{1}\,0\rangle$ basal and $\{0\,1\,\bar{1}\,0\}\langle 2\,\bar{1}\,\bar{1}\,0\rangle$ prism slip are not so much different from each other.

Fig. 8(c) compares the extrapolated bulk CRSS values for basal slip at room temperature obtained from the present micropillar compression tests with those obtained by high-temperature compression tests for bulk single crystals [8,9,17]. CRSS values for basal slip obtained by compression tests of bulk single crystals of 6*H*- and 4*H*–SiC have been reported to depend strongly on temperature and strain rate [8,9,17–19]. For various semiconducting materials with the diamond and zinc blende structures, the strain rate $\dot{\gamma}$ can be expressed generally as a function of CRSS $\tau_c$ and temperature $T$ with the following equation.

$$\dot{\gamma} \propto \tau_c^m \exp(-Q/kT), \tag{2}$$

where $m$ is the stress exponent and $k$ is the Boltzmann constant [8]. Fig. 8(c) shows the ln $\tau_c$ vs. $(1/T)$ plot for basal slip in 6*H*–SiC (strain rate: ~$10^{-4}$/s) previously reported [8,9,17]. Two fitting curves with different slopes intersect with each other at around 1100 °C, at which the transition in the thermal activation processes is considered to occur [17]. Detailed analysis of dislocation microstructures has suggested that basal slip occurs by two different deformation mechanisms depending on temperature; by (i) glide of completely dissociated $a/3\langle 1\,\bar{2}\,10\rangle$ dislocations and (ii) glide of single leading partial dislocations, above and below a critical transition temperature $T_c$ (~1100 °C for 6*H*–SiC deformed at a relatively slow strain rate of the order of $10^{-4}$ /s), respectively [17]. If the basal slip occurs at room temperature by the latter mechanism (ii) observed in bulk compression experiments below 1100 °C, the room temperature CRSS value is expected to be on the corresponding fitted line. However, the room-temperature bulk CRSS value deduced based on the present micropillar compression tests is found to be much lower than that extrapolated from the high-temperature data. This clearly indicates that the thermal activation mechanism for basal slip operated at room temperature for micropillar specimens is different from that operated below 1100 °C for bulk single crystals. In the micropillar specimen compressed at room temperature, we found that the majority of dislocations are perfect (undissociated) dislocations without exhibiting apparent dissociation at least at the resolution of weak-beam imaging. In addition, there exist some dissociated dislocations with an average separation distance much narrower than those observed after high-temperature deformation [12]. These observations suggest that perfect dislocations are nucleated in the shuffle set plane during loading and some of them cross-slip locally to dissociate in the glide set plane either during or after loading. The much narrower separation distance of these dissociated dislocations together with the existence of dislocation nodes formed by perfect and dissociated dislocations suggest that the cross-slip and subsequent dissociation events may occur as a result of post mortem structure relaxation during the unloading process from the high stress state, as previously deduced for Si, GaAs and 4*H*–SiC deformed under high confining pressure [13,15,20]. We thus conclude that the room-temperature CRSS value for basal slip deduced based on the present micropillar compression tests corresponds to the stress required to nucleate perfect dislocations in the shuffle set plane in the virgin specimen. This conclusion is further supported by the fact that basal dislocations (widely dissociated in the glide set plane) introduced by pre-straining at 1300 °C do not affect the CRSS values for basal slip in micropillar compression much, as shown in Fig. 8(a).

### 4.2. Dislocation nucleation during micropillar compression

In the case of single crystals of semiconducting materials such as Si, GaAs and SiC, the density of grown-in dislocations is generally quite low and therefore, it is highly probable that no dislocation is included in virgin micropillar specimens. Then, the nucleation of dislocations should occur during loading in micropillar compression tests most probably from the specimen surface. Bei et al. [48] applied the procedure proposed by Beltz and Freund [49] to explain the possible reason for the relatively low CRSS observed in their micropillar specimens of Mo when compared to the corresponding theoretical value and that deduced from the results of nanoindentation experiments. They attributed the relatively low CRSS to the heterogeneous nucleation of half or quarter dislocation loops at the surfaces or edges of micropillars [48]. We employ a similar analysis procedure to estimate the CRSS value for basal slip in 6*H*–SiC observed in micropillar specimens at room temperature. The self-energy of a half dislocation loop of a radius $r$ on the basal plane is expressed with the following equation.

$$E_{\text{half}} = \frac{K_s b^2 r}{8}\left(\frac{2-\bar{\nu}}{1-\bar{\nu}}\right)\ln\frac{8mr}{e^2 r_0}, \tag{3}$$

where $K_s$ and $r_0$ are the energy factor for a straight screw dislocation and the core cut-off radius, respectively [49,50–52]. The parameter $\bar{\nu}$, corresponding to Poisson's ratio for isotropic materials, is obtained by $\bar{\nu} = (K_e - K_s)/K_e$, where $K_e$ is the energy factor for a straight edge dislocation in the basal plane [50–52]. A geometry-dependent correction factor $m$ is estimated to be about 0.535 for a half dislocation loop on the basal plane using Eq. (17) in Ref. [49] with $\bar{\nu}$ = 0.216 estimated using the elastic constants of $c_{11}$ = 501, $c_{33}$ = 553, $c_{12}$ = 111, $c_{13}$ = 52, $c_{44}$ = 163 GPa [53]. The total energy change $U_{\text{half}}$ by the introduction of a half dislocation loop of a radius $r$ is estimated to be

$$U_{\text{half}} = E_{\text{half}} + E_{\text{ledge}} - W_{\text{stress}}, \tag{4}$$

where $E_{\text{ledge}}$ and $W_{\text{stress}}$ are the energy of the surface ledge formed by a half dislocation loop of a radius $r$ and the work done by the applied load, respectively [49]. The total energy change $U_{\text{half}}$, which is a function of the radius $r$ and applied shear stress $\tau$, takes a maximum value $U_{\max}$ at a critical radius of $r_c$. Similar analysis is made for the case of a

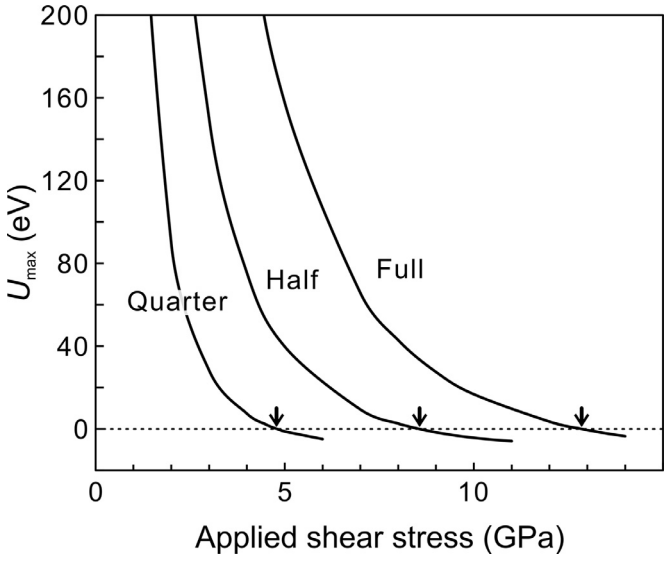


**Fig. 9.** Total energy change by nucleation of a basal dislocation loop from specimen surfaces (a half loop), edges (a quarter loop) and inside (a full loop) as a function of applied shear stress.

**Table 1**
Material parameters used for the estimation of the critical shear stress $\tau_{crit}$ for the spontaneous nucleation of a basal dislocation loop at 0 K (Fig. 8).

| $K_s$ (GPa) | $K_e$ (GPa) | $\bar{\nu}$ (GPa) | $b$ (nm) | Surface energy $\gamma_s$ (J/m$^2$)* |
|---|---|---|---|---|
| 178.3 | 227.4 | 0.216 | 0.308 | 1.71 |

Note: The surface energy $\gamma_s$ for (0001) basal plane is evaluated from the fracture toughness value $K_{IC}$ (= 1.37 MPa m$^{1/2}$) estimated in this study (Section 3.4) using the equation $\gamma_s = K_{IC}^2(1-\nu'^2)/(2E')$, where $E'$ and $\nu'$ are anisotropic Young's modulus (= 544.1 GPa) and Poisson's ratio (= 0.085) calculated based on the elastic constants reported in [53].

quarter dislocation loop with the assumption that the $m$ value is equal to 0.3 based on the discussion made by Bei et al. [48]. Fig. 9 shows the $U_{max}-\tau$ plots for half and quarter dislocation loops together with that for a full dislocation loop calculated with the core cut-off radius of $b$ and parameters summarized in Table. 1. The critical shear stress $\tau_{crit}$, above which the dislocation loop spontaneously expands at 0 K, can be estimated to be about 4.8, 8.6 and 12.9 GPa for quarter, half and full dislocation loops, respectively, from the $\tau$ value at which the $U_{max}$ value is equal to zero. The estimated $\tau_{crit}$ value for a quarter dislocation loop nucleation is in fairly good agreement with the room-temperature bulk CRSS value for basal slip deduced based on the results of micropillar compression tests. This indicates that the bulk CRSS values deduced in the present micropillar experiments are likely to correspond to the stress required to nucleate dislocations from the surface or edges of micropillar specimens. For micropillar specimens fabricated by the FIB method, the surface damage inevitably introduced during the FIB process could also affect the dislocation nucleation process. In the present case of 6$H$–SiC, the thickness of the surface amorphous layer introduced by the FIB milling was confirmed to be relatively thin (less than about 15 nm) compared to the edge length $L$ ranging from 1 to 7 $\mu$m of the micropillar specimens. In addition, the hardness and elastic modulus of ion-beam induced amorphous SiC have been reported to be lower than those of crystalline SiC [54–57]. Thus, we do believe that the FIB damage causes only a minor effect on the dislocation nucleation from the surface or edges of micropillar specimens. However, further experiments should be required to clarify the influence of the FIB damage.

The deformation behavior (CRSSs and stress–strain curves) by basal slip in micropillar compression is not affected by the existence of dislocations introduced by a high-temperature (1300 °C) deformation prior to micropillar compression. This is considered to originate from the fact that dislocations introduced at 1300 °C, which are widely dissociated dislocations gliding in the glide-set plane, do not move and consequently cannot act as dislocation sources in micropillar compression, while dislocations introduced and carry plastic strain during micropillar compression are perfect (undissociated) dislocations gliding in the shuffle-set plane. This is consistent with the results of theoretical calculation by Pizzagalli [58] that for dislocations with $\mathbf{b} = a/3[2\ \bar{1}\ \bar{1}\ 0]$ gliding on the basal plane in hexagonal 4$H$–SiC, the Peierls stress is lower for those in the shuffle-set (in the range of 9.4–9.5 GPa at zero K), while it is extremely high for those in the glide set so as to be sessile at zero K.

### 4.2. Plastic deformability of micropillar specimens

In the present study, we have successfully observed plastic flow in micropillar specimens of 6$H$–SiC single crystals at room temperature under a simple uniaxial compression condition, while the corresponding bulk single crystals do not exhibit any plastic flow under similar testing conditions. Premature fracture of brittle materials occurring in uniaxial compression has been discussed with many different models [59–62]. According to the model proposed by Ashby and his co-workers, premature fracture is assumed to occur by propagation of cracks that originate from pre-existing flaws in a direction parallel to the compression axis. The critical axial stress $\sigma_C$ for crack propagation is approximated to be $CK_{Ic}/(\pi a)^{1/2}$, where $a$ is a size of a pre-existing flaw and $C$ is a constant of the order of unity, depending on material, geometrical configuration and the number density of pre-existing flaws [60–62]. Fig. 10 plots the critical size of pre-existing flaws as a function of axial stress calculated with $K_{IC}$ values of 1.37 and 1.57 respectively for basal and prism plane cracking and $C$ = 1. The critical sizes of pre-existing flaws to avoid premature fracture under very high axial stress to activate basal and prism slip systems at room temperature are confirmed to be of the order of nanometers. Such tiny flaws are considered to be avoided in micropillar specimens, while they are inevitably included in bulk-sized specimens. Successful elimination of pre-existing flaws is considered to be the most probable reason why plastic flow is observed in micropillar specimens of 6$H$–SiC single crystals under uniaxial compression. Some other models to describe the brittle-to-ductile transition with respect to the specimen size in brittle materials have also been proposed [25,28].

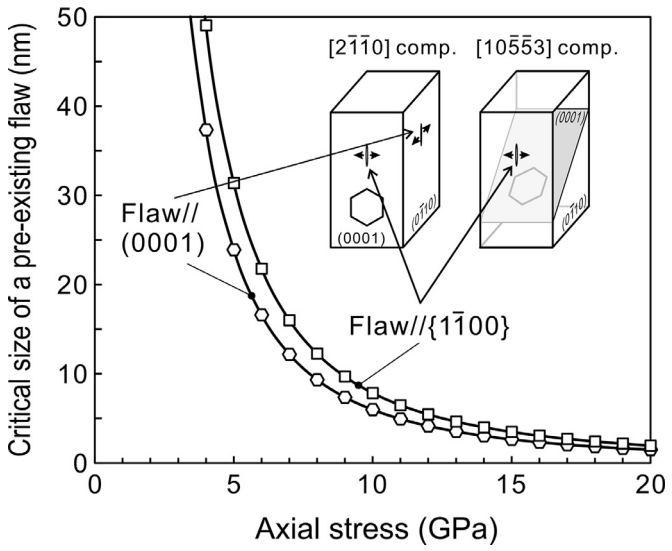


**Fig. 10.** Critical size of a pre-existing flaw that cause premature fracture as a function of axial stress.

## 5. Conclusions

The results of micropillar compression tests for 6$H$–SiC single crystals at room temperature are summarized as follows.

1. Basal and prism slip are operative at room temperature in 6$H$–SiC single crystals when the specimen size is reduced down to the micron-meter order, in contrast to the case of the corresponding bulk single crystals in which plastic flow by basal slip is observed above 550 °C. The CRSS values are very high (above 5 GPa) and exhibit "a smaller is stronger trend" following an inverse power-law relationship with a power-law exponent $n$ of ~0.10 and ~0.21 for basal and prism slip, respectively. The bulk CRSS values at room temperature are estimated to be 4.8 ± 1.0 and 4.5 ± 1.2 GPa for basal and prism slip, respectively.
2. Most dislocations with $\mathbf{b} = a/3[2\ \bar{1}\ \bar{1}\ 0]$ gliding on the basal plane tend to align along their screw orientation and glide as perfect (undissociated) dislocations during micropillar compression. Some of them are partly dissociated into two Schokley partials with the dissociation width in a range of 18–56 nm for 30° dislocations. The stacking fault energy on the basal plane is estimated to be 8–24 mJ/m$^2$, which is much higher than that (2.5 ± 0.9 mJ/m$^2$) estimated from

the dissociation width of dislocations introduced in the bulk 6*H*–SiC by high-temperature deformation (at 1520 °C) [12].

3. Dislocations with $\mathbf{b} = a/3[2\,\bar{1}\,\bar{1}\,0]$ gliding on the prism plane also exhibit a strong tendency to align along their screw orientation and glide as perfect (undissociated) dislocations during micropillar compression.
4. The deformation behavior (CRSSs and stress–strain curves) by basal slip in micropillar compression is not affected by the existence of dislocations introduced by a high-temperature (1300 °C) deformation prior to micropillar compression. This is because dislocations introduced at 1300 °C do not move and consequently cannot act as dislocation sources at room temperature in micropillar compression.
5. The values of fracture toughness $K_{IC}$ are estimated to be $1.37 \pm 0.13$ and $1.57 \pm 0.13$ MPa $m^{1/2}$ by three-point bend tests for chevron-notched single crystalline specimens with a notch plane being parallel to (0001) and $\{0\,1\,\bar{1}\,0\}$ planes, respectively.

## Declaration of Competing Interest

The authors declare that they have no known competing financial interests or personal relationships that could have appeared to influence the work reported in this paper.

## Acknowledgments

This work was supported by JSPS KAKENHI, Grant numbers JP18H01735, JP18H05478, JP18H05451, JP19H00824, the Elements Strategy Initiative for Structural Materials (ESISM) of MEXT, Grant number JPMXP0112101000, and in part by JST-ALCA, Grant Number JPMJAL1004.

## References

[1] W.D. Sylwestrowicz, Mechanical properties of single crystals of silicon, Philos. Mag. 7 (1962) 1825–1845.
[2] J.R. Patel, A.R. Chaudhuri, Macroscopic plastic properties of dislocation-free germanium and other semiconductor crystals. I. Yield behavior, J. Appl. Phys. 34 (1963) 2788–2799.
[3] R.L. Bell, W. Bonfield, The plastic deformation of germanium single crystals: yield and easy glide, Philos. Mag. 9 (1964) 9–36.
[4] D. Laister, G.M. Jenkins, Deformation of single crystals of gallium arsenide, J. Mater. Sci. 8 (1973) 1218–1232.
[5] A. George, J. Rabier, Dislocations and plasticity in semiconductors. I – dislocation structures and dynamics, Revue Phys. Appl. 22 (1987) 941–966.
[6] J. Rabier, A. George, Dislocation and plasticity. II – the relation between dislocation dynamics and plastic deformation, Revue Phys. Appl. 22 (1987) 1327–1351.
[7] P. Gall, J.P. Peyrade, R. Coquille, F. Reynaud, S. Gabillet, A. Albacete, Thermal activation of glide in INP single crystals, Acta Metall. 35 (1987) 143–148.
[8] S. Fujita, K. Maeda, S. Hyodo, Dislocation glide motion in 6H SiC single crystals subjected to high-temperature deformation, Philos. Mag. A 55 (1987) 203–215.
[9] A.V. Samant, P. Pirouz, Activation parameters for dislocation glide in $\alpha$-SiC, Int. J. Refract. Met. Hard Mater. 16 (1998) 277–289.
[10] V.G. Eremenko, V.I. Nikitenko, Electron microscope investigation of the microplastic deformation mechanicms of silicon by indentation, Phys. Stat. Sol. (a) 14 (1972) 317–330.
[11] M.J. Hill, D.J. Rowcliffe, Deformation of silicon at low temperatures, J. Mater. Sci. 9 (1974) 1569–1576.
[12] K. Maeda, K. Suzuki, S. Fujita, M. Ichihara, S. Hyodo, Defects in plastically deformed 6H SiC single crystals studied by transmission electron microscopy, Philos. Mag. A 57 (1988) 573–592.
[13] T. Suzuki, T. Yasutomi, T. Tokuoka, I. Yonenaga, Plastic deformation of GAAS at low temperatures, Philos. Mag. A 79 (1999) 2637–2654.
[14] J. Rabier, P. Cordier, J.L. Demenet, H. Garem, Plastic deformation of Si at low temperature under high confining pressure, Mater. Sci. Eng. A309–310 (2001) 74–77.
[15] H. Saka, K. Yamamoto, S. Arai, K. Kuroda, In-situ TEM observation of transformation of dislocations from shuffle to glide sets in Si under supersaturation of interstitials, Philos. Mag. 86 (2006) 4841–4850.
[16] J. Rabier, P.O. Renault, D. Eyidi, J.L. Demenet, J. Chen, H. Couvy, L. Wang, Plastic deformation of silicon between 20°C and 425°C, Phys. Stat. Sol. (c) 4 (2007) 3110–3114.
[17] A.V. Samant, W.L. Zhou, P. Pirouz, Effect of test temperature and strain rate on the yield stress of monocrystalline 6H–SiC, Phys. Stat. Sol. (a) 166 (1998) 155–169.
[18] J.L. Demenet, M.H. Hong, P. Pirouz, Plastic behavior of 4H–SiC single crystals deformed at low strain rates, Scr. Mater. 43 (2000) 865–870.
[19] A.V. Samant, M.H. Hong, P. Pirouz, The relationship between activation parameters and dislocation glide in 4H–SiC single crystals, Phys. Stat. Sol. (b) 222 (2000) 75–93.
[20] J.L. Demenet, X. Milhet, J. Rabier, TEM observations of the coexistence of perfect and dissociated dislocations in SiC under high stress, Phys. Stat. Sol. (c) 2 (2005) 1987–1991.
[21] J. Rabier, J.L. Demenet, On a change in deformation mechanism in silicon at very high stress: new evidences, Scr. Mater. 45 (2001) 1259–1265.
[22] M.D. Uchic, D.M. Dimiduk, J.N. Florando, W.D. Nix, Sample dimensions influence strength and crystal plasticity, Science 305 (2004) 986–989.
[23] J. Michler, K. Wasmer, S. Meier, F. Östlund, K. Leifer, Plastic deformation of gallium arsenide micropillars under uniaxial compression at room temperature, Appl. Phys. Lett. 90 (2007) 043123.
[24] B. Moser, K. Wasmer, L. Barbieri, J. Michler, Strength and fracture of Si micropillars: a new scanning electron microscopy-based micro-compression test, J. Mater. Res. 22 (2007) 1004–1011.
[25] W.W. Gerberich, J. Michler, W.M. Mook, R. Ghisleni, F. Östlund, D.D. Stauffer, R. Ballarini, Scale effects for strength, ductility, and toughness in "brittle" materials, J. Mater. Res. 24 (2009) 898–906.
[26] F. Östlund, K. Rzepiejewska-Malyska, K. Keifer, L.M. Hale, Y. Tang, R. Ballanini, W. Gerberich, J. Michler, Brittle-to-ductile transition in uniaxial compression of silicon pillars at room temperature, Adv. Funct. Mater. 19 (2009) 2439–2444.
[27] T.H. Sung, J.C. Huang, J.H. Hsu, S.R. Jian, Mechanical response of GAN film and micropillar under nanoindentation and microcompression, Appl. Phys. Lett. 97 (2010) 171904–1-3.
[28] F. Östlund, P.R. Howie, R. Ghisleni, S. Korte, K. Leifer, W.J. Clegg, J. Michler, Ductile-brittle transition in micropillar compression of GAAS at room temperature, Philos. Mag. 91 (2011) 1190–1199.
[29] S. Korte, W.J. Clegg, Discussion of the dependence of the effect of size on the yield stress in hard materials studied by microcompression of MgO, Philos. Mag. 91 (2011) 1150–1162.
[30] S. Korte, W.J. Clegg, Studying plasticity in hard and soft Nb-Co intermetallics, Adv. Eng. Mater. 14 (2012) 991–997.
[31] N. Takata, H. Ghassemi Armaki, Y. Terada, M. Takeyama, K.S. Kumar, Plastic deformation of the C14 laves phase $(Fe,Ni)_2Nb$, Scr. Mater. 68 (2013) 615–618.
[32] T. Csanádi, M. Bl'anda, A. Duszová, N.Q. Chinh, P. Szommer, J. Dusza, Deformation characteristics of WC micropillars, J. Eur. Ceram. Soc. 34 (2014) 4099–4103.
[33] J.J. Guo, K.M. Reddy, A. Hirata, T. Fujita, G.A. Gazonas, J.W. McCauley, M.W. Chen, Sample size induced brittle-to-ductile transition of single-crystal aluminum nitride, Acta Mater. 88 (2015) 252–259.
[34] T. Csanádi, P. Szommer, N.Q. Chinh, S. Grasso, J. Dusza, M. Reece, Plasticity in $ZrB_2$ micropillars induced by anomalous slip activation, J. Eur. Ceram. Soc. 36 (2016) 389–394.
[35] S. Korte-Kerzel, Microcompression of brittle and anisotropic crystals: recent advances and current challenges in studying plasticity in hard materials, MRS comm. 7 (2017) 109–120.
[36] N.L. Okamoto, D. Kashioka, M. Inomoto, H. Inui, H. Takebayashi, S. Yamaguchi, Compression deformability of $\Gamma$ and $\zeta$ Fe–Zn intermetallics to mitigate detachment of brittle intermetallic coating of galvannealed steels, Scr. Mater. 69 (2013) 307–310.
[37] N.L. Okamoto, M. Inomoto, H. Adachi, H. Takebayashi, H. Inui, Micropillar compression deformation of single crystals of the intermetallic compound $\zeta$-$FeZn_{13}$, Acta Mater. 65 (2014) 229–239.
[38] S. Nakatsuka, K. Kishida, H. Inui, Micropillar compression of $MoSi_2$ single crystals, MRS Symposium Proceedings, 1760, 2015. mrsf14-1760-yy05-09.
[39] K. Kishida, T. Maruyama, H. Matsunoshita, T. Fukuyama, H. Inui, Micropillar compression deformation of single crystals of $Mo_5SiB_2$ with the tetragonal $D8_l$ structure, Acta Mater. 159 (2018) 416–428.
[40] M. Higashi, S. Momono, K. Kishida, N.L. Okamoto, H. Inui, Anisotropic plastic deformation of single crystals of the MAX phase compound $Ti_3SiC_2$ investigated by micropillar compression, Acta Mater. 161 (2018) 161–170.
[41] S. Kiani, K.W.K. Leung, V. Radmilovic, A.M. Minor, J.-.M. Yang, D.H. Warner, S. Kodambaka, Dislocation glide-controlled room-temperature plasticity in 6H–SiC single crystals, Acta Mater. 80 (2014) 400–406.
[42] G. Kwon, H. Jo, S. Lim, C. Shin, H. Jin, J. Kwon, G. Sun, Room-temperature yield and fracture strength of single crystalline 6H silicon carbide, J. Mater. Sci. 50 (2015) 8104–8110.
[43] X. Deng, J. Bitler, K.K. Chawla, B.R. Patterson, Toughness measurement of cemented carbides with chevron-notched three-point bend test, Adv. Eng. Mater. 12 (2010) 948–952.
[44] G. Sernicola, T. Giovannini, P. Patel, J.R. Kermode, D.S. Balint, T.B. Britton, F. Giuliani, In situ stable crack growth at the micron scale, Nat. Commun. 18 (2017) 108 article number.
[45] H. Kitahara, Y. Noda, F. Yoshida, H. Nakashima, N. Shinohara, H. Abe, Mechanical behavior of single crystalline and polycrystalline silicon carbides evaluated by Vickers identaion, J. Cer. Soc. Jpn. 109 (2001) 602–606.
[46] D.M. Dimiduk, M.D. Uchic, T.A. Parthasarathy, Size-affected single-slip behavior of pure nickel microcrystals, Acta Mater. 53 (2005) 4065–4077.
[47] M.D. Uchic, P.A. Shade, D.M. Dimiduk, Plasticity of micrometer-scale single crystals in compression, Annu. Rev. Mater. Res. 39 (2009) 161–186.
[48] H. Bei, Y.F. Gao, S. Shim, E.P. George, G.M. Pharr, Strength differences arising from homogeneous versus heterogeneous dislocation nucleation, Phys. Rev. B 77 (2008) 060103-1–4.

[49] G.E. Beltz, L.B. Freund, On the nucleation of dislocations at a crystal surface, Phys. Stat. Sol. (b) 180 (1993) 303–313.
[50] Y.T. Chou, H.C. Yang, Equivalence between energy expression for dislocation loops in hexagonal and isotropic media, Philos. Mag. 28 (1973) 1003–1006.
[51] J.W. Steeds, Introduction to Anisotropic Elasticity Theory of Dislocations, Clarendon Press, Oxford, 1973.
[52] P.A. Anderson, J.P. Hirth, J. Lothe, Theory of Dislocations, 3rd. ed., Cambridge University Press, New York, 2017.
[53] K. Kamitani, M. Grimsditch, J.C. Nipko, C.-K. Loong, M. Okada, I. Kimura, The elastic constants of silicon carbide: a Brillouin-scattering study of 4H and 6H SiC single crystals, J. Appl. Phys. 82 (1997) 3152–3154.
[54] C.J. McHargue, D.L. Joslin, J.M. Williams, The hardness and elastic modulus of chromium-implanted silicon carbide, Nucl. Instrum. Methods Phys. Res. B 46 (1990) 185–188.
[55] W.J. Weber, N. Yu, L.M. Wang, N.J. Hess, Temperature and dose dependence of ion-beam-induced amorphization in – SiC, J. Nucl. Mater. 244 (1997) 258–265.
[56] W.J. Weber, L.M. Wang, N. Yu, N.J. Hess, Structure and properties of ion-beam-modified (6H) silicon carbide, Mater. Sci. Eng. A 253 (1998) 62–70.
[57] L.L. Snead, S.J. Zinkle, J.C. Hay, M.C. Osbourne, Amorphization of SiC under ion and neutron irradiation, Nucl. Instrum. Methods Phys. Res, B 141 (1998) 123–132.
[58] L. Pizzagalli, Stability and mobility of screw dislocations in 4H, 2H and 3C silicon carbide, Acta Mater. 78 (2014) 236–244.
[59] S. Nemat-Nasser, H. Horii, Compression-induced nonplanar crack extension with application to splitting exfoliation, and rockburst, J. Geophys. Res. 87 (1982) 6805–6821.
[60] M.F. Ashby, S.D. Hallam, The failure of brittle solids containing small cracks under compressive stress states, Acta Metall. 34 (1986) 497–510.
[61] C.G. Sammis, M.F. Ashby, The failure of brittle porous solids under compressive stress states, Acta Metall. 34 (1986) 511–526.
[62] M.F. Ashby, C.G. Sammis, The damage mechanics of brittle solids in compression, Pure Appl. Geophys. 133 (1990) 489–521.